Published in final edited form as:
Neuroimage. 2011 January 1; 54(1): 113–122. doi:10.1016/j.neuroimage.2010.08.033.

Regional differences in MRI detection of amyloid plaques in AD transgenic mouse brain

T.M. Wengenack[a], **D.A. Reyes**[b], **G.L. Curran**[a], **B.J. Borowski**[b], **J. Lin**[c], **G.M. Preboske**[b], **S.S. Holasek**[a], **E.J. Gilles**[a], **R. Chamberlain**[c], **M. Marjanska**[c], **C.R. Jack Jr.**[b], **M. Garwood**[c], and **J.F. Poduslo**[a,*]

[a]Molecular Neurobiology Laboratory, Departments of Neurology, Neuroscience, and Biochemistry/Molecular Biology, Mayo Clinic College of Medicine, Rochester, MN, 55905, USA

[b]Department of Radiology, Mayo Clinic College of Medicine, Rochester, MN, 55905, USA

[c]Center for Magnetic Resonance Research and Department of Radiology, University of Minnesota Medical School, Minneapolis, MN, 55455, USA

Abstract

Our laboratory and others have reported the ability to detect individual Alzheimer's disease (AD) amyloid plaques in transgenic mouse brain in vivo by magnetic resonance imaging (MRI). Since amyloid plaques contain iron, most MRI studies attempting to detect plaques in AD transgenic mouse brain have employed techniques that exploit the paramagnetic effect of iron and have had mixed results. In the present study, using five-way anatomic spatial co-registration of MR images with three different histological techniques, properties of amyloid plaques in AD transgenic mouse brain were revealed that may explain their variable visibility in gradient- and spin-echo MR images. The results demonstrate differences in the visibility of plaques in the cortex and hippocampus, compared to plaques in the thalamus, by the different MRI sequences. All plaques were equally detectable by T_2SE, while only thalamic plaques were reliably detectable by T_2*GE pulse sequences. Histology revealed that cortical/hippocampal plaques have low levels of iron while thalamic plaques have very high levels. However, the paramagnetic effect of iron does not appear to be the sole factor leading to the rapid decay of transverse magnetization (short T_2) in cortical/hippocampal plaques. Accordingly, MRI methods that rely less on iron magnetic susceptibility effect may be more successful for eventual human AD plaque MR imaging, particularly since human AD plaques more closely resemble the cortical and hippocampal plaques of AD transgenic mice than thalamic plaques.

Keywords

Alzheimer's disease; magnetic resonance imaging; iron; thioflavine S; amyloid-β

[*]**Corresponding Author:** Joseph F. Poduslo, Ph.D., Molecular Neurobiology Laboratory, Depts. of Neurology, Neuroscience, and Biochem./Molec. Biol., Mayo Clinic College of Medicine, Rochester, MN 55905, Phone: (507) 284-1784, Fax: (507) 284-3383, poduslo.joseph@mayo.edu.

Disclosure Statement: The authors have no actual or potential conflicts of interest.

Introduction

Recent studies in Alzheimer's disease (AD) transgenic mice and human AD tissue specimens have reported the ability to image AD amyloid plaques using magnetic resonance imaging (MRI) without the aid of a contrast enhancing agent (Benveniste et al., 1999; Helpern et al., 2004; Jack et al., 2004; Jack et al., 2005; Lee et al., 2004; Poduslo et al., 2002; Vanhoutte et al., 2005; Zhang et al., 2004). Our laboratory demonstrated the ability to detect amyloid plaques in T_2-weighted MR images of AD transgenic mouse brains ex vivo (Poduslo et al., 2002), as well as in vivo (Jack et al., 2004; Jack et al., 2005), without the aid of a contrast agent. The preferred mechanism to produce endogenous contrast for visualizing plaques is based on the differential decay rate of water signal in plaques versus surrounding brain tissue. This decay process, also known as "transverse relaxation", is described by a time constant (T_2 or T_2*) that depends on the type of pulse sequence (spin-echo and gradient-echo, respectively) used in acquiring the MR data. It has been proposed that the detectability of amyloid plaques in T_2- and T_2*-weighted MR images is due to the presence of iron in plaques (Benveniste et al., 1999; Jack et al., 2004; Jack et al., 2005; Lee et al., 2004; Vanhoutte et al., 2005) which decreases the relaxation time (both T_2 and T_2*) of the plaque water. This hypothesis is consistent with the observation that amyloid plaques appeared larger in T_2*-weighted gradient-echo images compared to T_2-weighted spin-echo images (Jack et al., 2004). This "blooming effect" on T_2*-weighted images is consistent with the static local susceptibility gradients produced by microscopic tissue iron which is a paramagnetic species (Jack et al., 2004).

The presence of iron in AD amyloid plaques, as well as other metals such as copper and zinc, has been reported previously using histological and analytical methods (Falangola et al., 2005; LeVine, 1997; Lovell et al., 1998; Miller et al., 2006). High concentrations of iron and other metals in plaques are hypothesized to cause oxidative stress and generate free radicals that promote neurotoxicity and lead to neurodegeneration in AD (Gerlach et al., 1994; Smith and Perry, 1995). Iron, copper, and zinc have also been shown to promote the aggregation of amyloid peptides into fibrils (Huang et al., 2004). In normal human and rodent brain, high levels of iron are observed in regions including the basal ganglia (globus pallidus, caudate, and putamen), thalamic nuclei, substantia nigra, and red nucleus (Hill and Switzer, 1984; Koeppen, 1995; LeVine, 1991; Vymazal et al., 1995; Mitsumori et al., 2007). These structures exhibit accelerated T_2 and T_2* relaxation rates compared to other brain tissue, which is attributed to their high iron content (Schenck, 1995; Vymazal et al., 1995; Mitsumori et al., 2007). The high levels of iron in the substantia nigra have been proposed to play a role in Parkinson's disease pathogenesis by increasing oxidative stress and generating free radicals (Gerlach et al., 1994).

By using a modified Prussian blue iron staining technique that is more sensitive and involves the use of diaminobenzidine (DAB), oligodendrocytes and myelin sheaths have been shown to contain high concentrations of iron, particularly in the caudate putamen (LeVine, 1991) and thalamus (Hill and Switzer, 1984) of normal, wild-type mice or rats, which we have also observed in our wild-type mice (Jack et al., 2005). When using the same iron staining technique, our laboratory and others have recently observed that amyloid deposits in the cortex, hippocampus, and thalamus of AD transgenic mice, which are detectable by MRI, also stain positive for iron (Falangola et al., 2005; Jack et al., 2004; Jack et al., 2005; Lee et al., 2004; Vanhoutte et al., 2005). Our laboratory was able to perform positive four-way spatial correlations between in vivo T_2-weighted MRI, ex vivo T_2-weighted MRI, thioflavine S amyloid staining, and DAB-enhanced iron staining (Jack et al., 2005). In an earlier study, we observed that the large amyloid deposits in the thalamus of older APP/PS1 AD transgenic mice (~20 months) were particularly susceptible to T_2*-weighted MRI enhancement of their apparent size compared to T_2-weighted MRI and thioflavine S staining, suggesting they might contain high levels of iron (Jack et al., 2004). Histochemical staining for iron using the Prussian

blue reaction without DAB-enhancement stained thalamic plaques very intensely while cortical and hippocampal plaques stained very weakly, verifying that the thalamic plaques contained higher iron content (Jack et al., 2004). We subsequently used the more sensitive Prussian blue reaction with DAB enhancement to demonstrate that the cortical and hippocampal plaques also contain iron, but at much lower levels than the thalamic plaques (Jack et al., 2005). The purpose of the present study was to further characterize the cortical, hippocampal, and particularly the thalamic plaques using additional MRI sequences and tissue staining methods. MRI methods included T_2-weighted spin-echo (*T_2SE*) and T_2*-weighted gradient-echo (*T_2*GE*) pulse sequences. Tissue staining methods included DAB-enhanced iron staining, thioflavine S amyloid staining, and anti-Aβ immunohistochemistry. We specifically evaluated differences in iron content between cortical/hippocampal plaques and thalamic plaques. We determined that thalamic plaques contain amyloid-β peptide (Aβ), but are qualitatively different from cortical and hippocampal plaques. Densitometry was also performed on histological sections stained for iron to quantify the relative iron content of plaques compared to tissue in the same three brain regions.

Materials and methods

Animals

These experiments were performed using transgenic mice that express two mutant human proteins associated with familial AD and have been described in detail elsewhere (Holcomb et al., 1998). Hemizygous transgenic mice (Tg2576) expressing mutant human amyloid precursor protein (APP_{695}) (Hsiao et al., 1996) were mated with a strain of homozygous transgenic mice (M146L6.2) expressing mutant human presenilin 1 (PS1) (Holcomb et al., 1998). The animals were genotyped for the expression of both transgenes by a PCR method using a sample of mouse-tail DNA. Wild-type, non-transgenic (WT) mice were obtained from Jackson Labs (Strain B6SJLF1/J, Bar Harbor, ME) and were used as the background strain for the transgenic mice. The mice were housed in a virus-free barrier facility under a 12-hr light/dark cycle, with ad libitum access to food and water. All procedures performed were in accordance with the NIH Guidelines for the Care and Use of Laboratory Animals using protocols approved by the Mayo Clinic and University of Minnesota Institutional Animal Care and Use Committees.

Magnetic resonance imaging

APP/PS1 transgenic AD mice (9, 12, 24, and 30 months) were used in this study. MRI was performed ex vivo on perfused, formalin-fixed brains soaked in phosphate-buffered saline (PBS). After an overdose of sodium pentobarbital (200 mg/kg, IP), the animals were perfused with phosphate-buffered saline followed by neutral-buffered, 10% formalin. Each brain was removed and fixed further in formalin overnight and then immersed in PBS, pH 7.4 for 24 hours to remove excess formalin and equilibrate the brain in an isotonic solution. Each brain was then embedded vertically in 2% agar in a 15 mm-diameter glass tube. Ex vivo MRI was performed with a Unity Inova spectrometer (Varian, Palo Alto, CA) which was interfaced to a 9.4T/31 cm horizontal bore magnet equipped with actively-shielded gradients capable of 300 mT/m in a rise-time of 500 μs (Magnex Scientific, Abingdon, UK). Radiofrequency transmission and signal reception were performed with a dual-loop quadrature surface coil built in-house (loop diameter = 1 cm).

Mouse brains were imaged ex vivo with a T_2-weighted spin-echo (*T_2SE*) sequence designed specifically for this type of application and has been described previously (Jack et al., 2004). Imaging parameters were: repetition time (TR) = 2000 ms; echo time (TE) = 52 ms; image matrix size = 256 × 96 × 32 in the x, y, and z directions, respectively, at corresponding field-of-view (FOV) of 15.36 mm × 5.76 mm × 3.84 mm, which resulted in nominal voxel

dimensions of 60 μm × 60 μm × 120 μm. Acquisition time using the T_2SE sequence was 1 hr., 42 min. These are the same pulse sequence parameters which we successfully used to detect individual amyloid plaques in APP/PS1 mice in vivo (Jack et al., 2004; Jack et al., 2005). The brains were also scanned with a 3D T_2*-weighted gradient-echo (T_2*GE) sequence to maximize the relaxivity of endogenous iron. The T_2*GE sequence parameters were: TR = 150 msec, TE = 16.4 msec, nominal flip angle = 15°, acquisition bandwidth = 60 kHz; image matrix size = 256 × 256 × 128 in the x, y, and z directions, respectively, with a corresponding FOV of 15.36 mm × 15.36 mm × 3.84 mm. This resulted in nominal voxel dimensions of 60 μm × 60 μm × 120 μm, respectively. Acquisition time was 1 hr., 22 min. MR images were filtered to smooth noise while preserving edges.

Histological techniques

After ex vivo MRI was completed, brains were removed from the agar and processed histologically. A 5-mm thick block of agar was left attached to the posterior of the hemisphere as a base for mounting to the microtome platform in order to maintain the same orientation of the hemisphere as in the MRI scan. After cryoprotecting for 24 hrs. each in 10% and then 30% sucrose in 0.1 M phosphate, pH 7.4, frozen coronal sections (30 μm) were cut with a sliding microtome throughout the whole extent of the cerebral cortex. The brains were sectioned in the same coronal orientation histologically as in the MRI scan. Adjacent 30 μm sections were processed histochemically for the presence of iron or stained with thioflavine S or anti-Aβ immunohistochemistry (IH) to detect amyloid deposits.

In order to visualize tissue iron, a diaminobenzidine (DAB)-enhanced method of the Prussian blue reaction was performed that is sensitive enough to detect trace amounts of iron in AD plaques (LeVine, 1991; LeVine, 1997). Briefly, mounted 30-μm sections were rehydrated in PBS and then incubated in 10 mg/ml sodium borohydride (Sigma Chemical, St. Louis, MO) in PBS for 30 min. The sections were washed twice for 5 min. between each step in PBS. The sections were incubated for 20 min. in 30 μg/ml proteinase K (Sigma Chemical, St. Louis, MO), 0.1% Triton X in PBS. The sections were then incubated in 1% potassium ferrocyanide (Sigma Chemical, St. Louis, MO), 1% HCl, and 1% Triton X in distilled water for 30 min. Lastly, the sections were incubated in 0.5 mg/ml 3,3'-diaminobenzidine tetrahydrochloride (Sigma Chemical, St. Louis, MO) and 2 μl/ml 30% hydrogen peroxide (Sigma Chemical, St. Louis, MO) in 0.05 M Tris HCl, pH 7.6, for 15 min. in the dark. The sections were rinsed for five minutes each in three changes of distilled water, dehydrated, coverslipped, and then imaged without counterstaining. In negative control sections in which the potassium ferrocyanide step was omitted but the DAB/H_2O_2 step was included to test for the presence of endogenous peroxidases, no plaques were stained, confirming the specificity of the staining for iron and its presence in plaques.

The other two sets of adjacent sections were processed histologically to detect amyloid deposits and plaques using two standard methods. One set of sections was mounted and stained with fresh, filtered, aqueous 1% thioflavine S using a standard protocol (Wengenack et al., 2000). The thioflavine S positive amyloid plaques were visualized with epifluorescence microscopy using filters for fluorescein isothiocyanate (excitation = 488 nm; emission = 520 nm). Another set of adjacent sections underwent IH for amyloid using a standard anti-Aβ monoclonal mouse antibody (4G8, Covance Research Products, Berkeley, CA). Briefly, free-floating sections were washed with PBS/0.3% Triton-X (PBST). Endogenous peroxidase activity in the sections was quenched by reacting with 0.5% H_2O_2 in PBST for 30 min. The sections were blocked with 1.5% normal horse serum in TBS for 60 min. The sections were incubated with the anti-Aβ primary antibody at a dilution of 1:1000 in 0.1% BSA/0.3% Triton-X/PBS overnight at 4° C. The primary antibody was then visualized using a Vectastain Elite ABC immunoperoxidase

kit (PK-6102) and Vector VIP (SK-4600) as the substrate according to the instructions (Vector Laboratories, Burlingame, CA).

Anatomic matching of MR images to histological sections

Anatomic spatial co-registration between T_2SE and T_2*GE MRI scans and the corresponding histological sections of the same mouse was accomplished using image analysis software with a linked cursor system (Analyze, Analyze Direct, Overland Park, KS) (Robb, 1990). Using the iron-stained histological section as the reference section, the spatially matched ex vivo MRI (virtual) section was determined using readily identifiable anatomic landmarks common to both sections such as the hippocampus, white matter tracts, and blood vessels. If necessary, the MRI volume was rotated on the x or y axis to compensate for slight changes in orientation that may have occurred transferring the brain from the agar to the microtome. The occurrence of the same plaque in both the histological and MRI section was verified using the linked-cursor tool.

Densitometry of plaques and tissue in APP/PS1 and WT brain sections stained for iron

The relative iron content of plaques in cortex, hippocampus, and thalamus was determined by densitometry of the histological sections stained for iron with the DAB-enhanced Prussian blue method. Using grayscale images, the mean gray level intensity was measured in ten plaques in each region of a 24-month old APP/PS1 mouse brain and an age-matched WT mouse. The mean intensity of tissue was also measured in a plaque-free, 20-pixel^2 ROI adjacent to each plaque and corresponding locations in the WT brain images. All histochemical conditions, as well as microscope and camera settings were kept constant between APP/PS1 and WT brain sections. Statistical analysis was performed by a two-way ANOVA of plaque versus tissue intensity across three brain regions followed by Student-Newman-Keuls post-hoc multiple comparisons (Sigma Stat 3.10, Systat Software, San Jose, CA).

Total iron content of brain tissue in APP/PS1 and WT mice

Total iron content of brain tissue in APP/PS1 and WT mice was measured in fresh, PBS-perfused, frozen tissue from cortex, hippocampus, and thalamus using inductively coupled plasma – mass spectrometry (ICP-MS). Samples from 24-month old mice were tested following acid digestion. Results were reported as μg iron/g tissue. Statistical analysis was performed by a two-way ANOVA of APP/PS1 versus WT brain tissue iron across three brain regions followed by Student-Newman-Keuls post-hoc multiple comparisons (Sigma Stat 3.10, Systat Software, San Jose, CA).

Results

Five-way spatial co-registration of plaques in cortex, hippocampus, and thalamus

The purpose of the present study was to further investigate the role of iron in the detectability of AD amyloid plaques by MRI. The results are illustrated in Figures 1–4 which show five-way spatially co-registered MR images of ex vivo scans using T_2SE or T_2*GE sequences in brains from AD transgenic mice at 9, 12, 24, or 30 months of age and corresponding histological sections stained for iron, thioflavine S, or anti-Aβ IH, respectively. The results indicated that all amyloid plaques contained some iron. Spatial co-registration of individual plaques was not performed in the 9-month old mouse (Fig. 1) because the plaques were not large enough so that the same plaques could be observed in all three adjacent histological sections. However, we have previously performed four-way spatial co-registration between in vivo T_2SE, ex vivo T_2SE, thioflavine S, and iron stained sections in mice as young as 6 and 9 months (Jack et al., 2005). No WT mice have displayed amyloid or iron-containing deposits at the ages studied (3–24 months) thus far in our laboratory (not shown). The appearance of MR images and

histological sections stained with thioflavine S or for iron from WT mice can be seen in our previous reports (Jack et al., 2004; Jack et al., 2005). As we have reported previously, we are able to consistently detect individual AD amyloid plaques by MRI both ex vivo and in vivo in APP/PS1 transgenic mouse brain, confirmed by spatial co-registration to histological sections, without the aid of a contrast-enhancing agent (Jack et al., 2004; Jack et al., 2005).

In the present study, many plaques were detectable by MRI in the cortex, hippocampus, and thalamus of ex vivo AD transgenic mouse brains, and they increased in frequency and size with age, as is also observed histologically (Wengenack et al., 2000). Plaques, particularly in the thalamus, could be detected with both T_2- and T_2*-weighted MRI, although more reliably in mice 12 months and older (e.g., Figs. 4A, 4C, 4D, 4F). While cortical and hippocampal plaques start to develop around 3 months of age in APP/PS1 mice (Wengenack et al., 2000), plaques do not generally appear in the thalamus until around 12 months of age, which will be discussed more in the next paragraph. In T_2-weighted images, plaques in the cortex and hippocampus appeared with similar conspicuity as the thalamic plaques, but were less obvious in the T_2*-weighted images (e.g., Figs. 4A, 4B, 4D, 4E). In T_2-weighted images, all plaques appeared to be approximately the same size as they were in the histological sections. In T_2*-weighted images, however, the thalamic plaques appeared to be much larger and more hypointense than in the T_2-weighted images, most likely due to the magnetic susceptibility effect of iron which has its greatest effect on T_2*-weighted images (compare Figs. 3C and 4C to 3F and 4F, respectively). Quantitative measurements with image analysis revealed that the thalamic plaques were an average of 66% larger in diameter in T_2*-weighted images than in the three histological preparations, while the thalamic plaque diameters were only 3% larger in T_2-weighted images. The quantitative measurements also revealed, however, that the diameters of the cortical and hippocampal plaques were actually slightly larger in both the T_2*-weighted images (28%) and the T_2-weighted images (32%) compared to their diameters in the three histological preparations. Image analysis of plaque intensity in the MR images confirmed that the thalamic plaques were darker (by 30.5%) in T_2*-weighted images compared to T_2-weighted images. However, cortical and hippocampal plaques were actually brighter (by 17.4%) in T_2*-weighted images compared to T_2-weighted images, making them less conspicuous in T_2*-weighted images.

Histological analysis revealed that the plaques detectable by MRI could be divided into two populations based on their differing iron content and morphology. Cortical and hippocampal plaques contained low amounts of iron that could only be detected with a more sensitive technique, namely the DAB-enhanced Prussian blue method, while thalamic plaques contained much higher amounts of iron because they stained very intensely with the DAB-enhanced Prussian blue method and could also be detected with the less-sensitive Prussian blue method without DAB-enhancement (i.e., Perls' stain), as we have shown previously (Jack et al., 2004). Both populations of plaques stained with thioflavine S and contained Aβ peptide, as revealed by anti-Aβ IH. However, the morphology of the plaques was somewhat different. All cortical/hippocampal plaques had a fibrillar morphology, with an intensely thioflavine S-stained core and fibrils radiating out from it (Figs. 2K, 3K, 4K). Most thalamic plaques had a spherical morphology with a well-defined margin and no radiating fibrils (Figs. 2L, 3L, 4L). The thalamic plaques stained very intensely for iron throughout (Figs. 3F, 4F). Thioflavine S, however, stained the thalamic plaques non-uniformly, with intense staining around the perimeter and less intense staining in the core, giving a somewhat hollow appearance compared to the cortical/hippocampal plaques (Figs. 3L, 4L). Both types of plaques, however, were immunopositive to the standard anti-Aβ antibody, 4G8, displaying equal staining intensity throughout the whole plaque (Figs. 3N, 3O, 4N, 4O).

In summary, amyloid plaques detectable by MRI could be divided into two populations based on histological analysis and morphology. The two populations exhibited different levels of

detectability with the gradient-echo and spin-echo sequences. Thalamic plaques contained very high levels of iron and were detectable by both types of pulse sequences. The presence of thalamic plaques became more obvious with age due to the large magnetic susceptibility of the iron-laden plaques and the consequent "blooming" effect in T_2*–weighted images. As compared with the thalamic plaques, cortical/hippocampal plaques contained lower levels of iron, which is consistent with their reduced conspicuity (relative to thalamic plaques) in the T_2*–weighted images. On the other hand, cortical/hippocampal plaques displayed similar conspicuity as thalamic plaques in T_2-weighted images, because the spin-echo sequence compensated destructive interferences arising in the "static dephasing regime" (Yablonskiy and Haacke, 1994).

Densitometry of plaques and tissue in APP/PS1 brain sections stained for iron

Quantitative densitometry of brain sections from a 24-month old APP/PS1 mouse stained with the DAB-enhanced Prussian blue method for iron was used as a relative measure of iron content within plaques and tissue. Lower intensity values correspond to darker, more intense staining as a result of higher iron content oxidizing greater amounts of diaminobenzidine. This results in an inverse relationship between intensity level (brightness) and relative iron content because the densitometry intensity values are gray scale values where 0 equals pure black and 255 equals pure white. The results are listed in Table 1. Plaques in all three brain regions had significantly lower intensity values than adjacent tissue ($p<0.001$), indicating that plaques have relatively higher iron content. Among brain regions, the intensity value for thalamic plaques was more than ten fold lower than the intensity values for cortical or hippocampal plaques, indicating that thalamic plaques have much higher relative iron content. These quantitative densitometric results confirm the observations made above, whereby intensely dark staining of thalamic plaques in histological sections stained with the DAB-enhance Prussian blue method indicated very high relative levels of iron. In WT brain tissue, intensity values were slightly lower than APP/PS1 tissue free of plaques. While there was an overall significant difference by ANOVA ($p<0.001$), only the intensity values in the thalamus were significantly lower in WT compared to APP/PS1 ($p<0.001$). Across brain regions, the intensity values were significantly lower in the thalamus than the cortex in both APP/PS1 and WT mice ($p<0.001$). This indicates that thalamic tissue has relatively higher endogenous levels of iron and may be the source for higher iron levels in thalamic plaques compared to cortical or hippocampal plaques in APP/PS1 mice.

Total iron content of brain tissue in APP/PS1 and WT mice

Total iron content of brain tissue in 24-month old APP/PS1 and WT mice was measured in fresh, PBS-perfused, frozen tissue from cortex, hippocampus, and thalamus using inductively coupled plasma – mass spectrometry (ICP-MS). The results are listed in Table 2. Total iron content was higher in all three brain regions of APP/PS1 brain, compared to WT brain, with the highest concentration occurring in the thalamus. Statistical analysis performed by a two-way ANOVA of APP/PS1 versus WT brain tissue iron across three brain regions indicated that there were significantly higher levels of iron in APP/PS1 mouse brain (APP/PS1 vs. WT – [$F(1,11)=18.04$, $p<0.005$]; Brain Region – [$F(2,11)=4.27$, $p<0.07$]; APP/PS1 vs. WT × Region Interaction – [$F(2,11)=2.65$, ns]). Student-Newman-Keuls post-hoc multiple comparisons indicated that only the iron content of the thalamus reached a level of statistical significance. This chemical analysis reveals that the overall iron content of the APP/PS1 mouse brain is higher than in WT mice, particularly in the thalamus.

Discussion

Putative mechanisms of plaque detectability

Due to the greater conspicuity of cortical and hippocampal plaques in T_2- versus T_2*-weighted images and relative to the thalamic plaques in young AD mice, we originally believed that two mechanisms might be responsible for the MRI signal loss associated with amyloid plaques. One mechanism was transverse relaxation in the “dynamic dephasing regime”, which occurs due to water diffusion in microscopic magnetic field gradients in the time (TE) which elapses between excitation and the spin echo. The second mechanism was exclusion of tissue water protons from the dense hydrophobic core of larger amyloid plaques. A recent study from our laboratory, however, found that the water proton density of cortical plaques is only slightly lower than the surrounding tissue, while plaque T_2* and T_2 values were similar (Chamberlain et al., 2009). Thus, in spin-echo imaging of cortical and hippocampal plaques, other relaxation channels such as proton exchange and dipole-dipole interactions must also play a role, particularly for plaques that do not contain high levels of iron. Spin-echo sequences have been shown to be more sensitive to microscopic field gradients, whereas gradient-echo sequences are more sensitive to magnetic field gradients extending over much larger spatial scales (Fujita, 2001). When iron is present, T_2*-weighted sequences generally result in greater signal loss and spatial blooming, and as such, yield greater sensitivity for iron than T_2-weighted sequences. Cortical/hippocampal plaques, however, did not exhibit the susceptibility “blooming” effect that was observed around the thalamic plaques. Iron in cortical and hippocampal plaques may therefore exist in a form and distribution that produces only microscopic susceptibility gradients. Although we used a surface coil in this study, we do not believe the results are attributable to decreases in MR signal with increased distance from the coil. While gradient echo sequences may be more sensitive to MR signal decrease, it should not alter the tissue contrast characteristics because we previously found that the T1 values of amyloid plaques and surrounding tissue are similar (Chamberlain et al., 2009). We observed much greater magnetic susceptibility effects in thalamic plaques, which are farther from the coil, than in cortical or hippocampal plaques. One might expect the opposite to be the case if depth sensitivity of the surface coil was a major contributing factor to the results.

Previous MRI studies

Previously, using a four-way anatomic spatial co-registration of in vivo T_2SE MRI with ex vivo T_2SE MRI, thioflavine S histological staining, and DAB-enhanced iron histological staining, we reported that individual amyloid plaques were not only detectable in vivo by MRI without the aid of a contrast enhancing agent in AD transgenic mice, but that they also contain iron (Jack et al., 2005). One other study was also able to detect individual plaques in vivo by MRI without the aid of a contrast agent (Vanhoutte et al., 2005). That study used T_2*GE pulse sequences and was able to detect thalamic plaques, but not cortical/hippocampal plaques, reporting the same results in vivo that we observed ex vivo in relation to thalamic plaques, their iron content, and visibility by T_2*-weighted pulse sequences (Vanhoutte et al., 2005). Another study was able to detect cortical/hippocampal plaques in vivo by MRI using a T_2*-weighted pulse sequence with the aid of a contrast agent, but only after administration of mannitol to transiently open the blood-brain barrier (Wadghiri et al., 2003). Earlier studies that employed T_2*-weighted pulse sequences to detect amyloid plaques ex vivo had mixed results (Benveniste et al., 1999; Dhenain et al., 2002). Several other studies have reported the ability to detect individual plaques by ex vivo MRI with and without the aid of a contrast agent (Lee et al., 2004; Poduslo et al., 2002; Wadghiri et al., 2003; Zhang et al., 2004).

Comparison of pulse sequences

The present study compared two types of pulse sequences (T_2SE and T_2*GE) side by side in one experiment using five-way anatomic spatial co-registration with histological staining for

iron, thioflavine S, and anti-Aβ IH to determine the relative detectability of amyloid plaques with different pulse sequences. This side-by-side analysis allowed us to compare the detectability of different types of amyloid plaques by different MR pulse sequences. Plaques in the thalamus were detectable by both pulse sequences, but plaques in the cortex and hippocampus were reliably detectable by only the T_2SE pulse sequence in the present study. Thalamic plaques contained very high levels of iron, while cortical/hippocampal plaques contained much lower levels of iron. Iron played a large role in the detectability of thalamic plaques because they appeared larger than their true size and increased in apparent size with increasing TE, as observed by us, as well as others, thus confirming the magnetic susceptibility effects of iron (Vanhoutte et al., 2005). However, in our experience, cortical and hippocampal plaques are less conspicuous than thalamic plaques when using the T_2*GE sequence. As discussed above, this observation can be explained by lower iron content in cortical and hippocampal plaques as compared with thalamic plaques. It can also be partially due to the shorter TE of the T_2*GE sequence, which must be used to minimize image artifacts (i.e., signal dropout) arising from bulk magnetic susceptibility effects. While plaque size was definitely a factor in the overall detectability of plaques and thalamic plaques were generally larger than cortical/hippocampal plaques, there was no apparent correlation of iron content with plaque size. Iron content was more dependent on plaque morphology, such that all (spherical) thalamic plaques had very high iron content and all (fibrillar) cortical/hippocampal plaques had very low iron content regardless of size, with no similarity or overlap in iron content among plaques of similar size between the two types.

This suggested that some other factor contributed to the detectability of cortical/hippocampal plaques by T_2SE pulse sequences. Since cortical/hippocampal plaques have very dense, hydrophobic, crystalline cores that stain very intensely with thioflavine S, water exclusion was originally believed to play a larger role than iron in the detectability of cortical/hippocampal plaques by T_2SE pulse sequences. Higher levels of vascularity in the cortex and hippocampus might result in higher water content in those regions compared to the thalamus. However, proton density measurements indicated that there was no difference in water content between plaques and surrounding tissue (Chamberlain et al., 2009). Furthermore, since we observed the same profile of plaque detectability both in vivo and ex vivo among the pulse sequences and the regional water content could differ greatly between in vivo and ex vivo specimens, differences in water content most likely do not play a significant role in regional differences in plaque detectability. Regardless, since T_2SE pulse sequences not only impart equal detectability of most plaques (cortical/hippocampal and thalamic), with the noted exception of diffuse plaques, but also give an accurate representation of their size independent of their iron content, pulse sequences that rely less on iron paramagnetic effects should be employed for use in in vivo MRI plaque detection in developmental studies of plaque deposition or therapeutic studies of plaque prevention/removal by secretase inhibitors or passive immunization.

Regional differences in iron

The main reason it is more desirable to be able to detect cortical/hippocampal plaques in AD transgenic mice rather than thalamic plaques is because they more closely resemble amyloid plaques in human AD patients and because an in vivo diagnostic imaging technique for AD in human patients is the ultimate goal of AD transgenic mouse MRI studies. However, the differences in iron content and morphology between cortical/hippocampal plaques and thalamic plaques present a unique opportunity to study the causes of plaque detectability by MRI. Since both types of plaques are immunoreactive for Aβ peptide, why do they exhibit such large differences in iron content? One explanation could simply be higher endogenous levels of iron in the surrounding tissue. Using DAB-enhanced iron staining, higher levels of iron, found predominantly in oligodendrocytes, have been reported to occur in white matter

tracts, such as the corpus callosum and fiber bundles running through the thalamus, in normal rats (Hill and Switzer, 1984). We have also observed similar patterns of iron staining in our WT mice (Jack et al., 2005). The posterior and ventral posteromedial thalamic nuclei, the regions in which the thalamic plaques are observed, have high levels of metabolic activity due to their high levels of cytochrome oxidase (Haidarliu and Ahissar, 2001). The cytochrome oxidase activity is highest in punctate regions referred to as the "whisker barreloids", which are responsible for processing sensory information from the vibrissae (Haidarliu and Ahissar, 2001). High levels of iron together with high metabolic activity suggest that these regions are very likely subjected to high levels of oxidative stress. Because it has been demonstrated in vitro that iron and other metals catalyze the aggregation of Aβ into fibrils and plaques (Mantyh et al., 1993), the higher levels of endogenous iron could also facilitate the formation of the thalamic plaques. However, because thalamic plaques appear in APP/PS1 mouse brain at a later age than cortical/hippocampal plaques (12 months vs. 3 months), other factors must also play a role in their formation. For example, the levels of transgene expression in the brain exhibit regional differences in this and other transgenic mouse models. The level of mutant APP transgene expression in the APP/PS1 mouse model is higher in the cortex and hippocampus than in the thalamus (Irizarry et al., 2001), while the level of PS1 transgene expression is higher in the posterior and ventral posteromedial thalamic nuclei than the cortex and hippocampus, with the exception of the CA3 region of the hippocampus (McGowan et al., 1999). Therefore, since Aβ peptide production is higher in the cortex and hippocampus, it would stand to reason that amyloid plaques would be more numerous in those regions.

Etiology of thalamic plaques

Since the cores of the thalamic plaques do indeed contain Aβ, some other factor must be responsible for their irregular thioflavine S staining. The spherical (thalamic) plaques develop at a much later age than the fibrillar plaques in the cortex and hippocampus, appearing at around 12 months of age, compared to about 3 months for fibrillar (cortical/hippocampal) plaques. Some fibrillar plaques were also observed in the thalamus at younger ages along with those in the cortex and hippocampus. The spherical thalamic plaques seemed to have a limited anatomical distribution. They were observed only in a few specific thalamic nuclei ventral to the dorsal hippocampus approximately between Bregma –1.0 to –2.5, which included the ventrolateral, the ventral posteromedial, and posterior thalamic nuclei, and were never observed in the cortex or hippocampus. The fibrillar plaques most closely resemble typical AD plaques in humans and generally do not have a regional preference in APP/PS1 mice, particularly with increasing age, although they are more prevalent in the cortex (all regions) and hippocampus than the midbrain, brainstem, and cerebellum.

Spherical amyloid deposits similar to those observed in the thalamus in the present study have also been reported in the antero-ventral nucleus of the thalamus in human AD patients (Braak and Braak, 1991). However, iron staining was not performed so the iron content of the deposits was not reported to determine if the deposits observed in AD brain are exactly the same as those observed in the AD transgenic mice. Similar deposits have also been reported to occur in normal human brain which were verified to contain iron by a DAB-enhanced Prussian blue iron staining method (Morris et al., 1992), as well as in the globus pallidus of non-human primates (Schultz et al., 2001; Wadsworth et al., 1995; Yanai et al., 1994). Spherical, globular "concretions" containing high levels of iron and very closely resembling those described here were observed in the globus pallidus and choroid plexus of normal human brain (Morris et al., 1992). Recent preliminary reports have also reported that thalamic plaques in AD transgenic mouse brain also contain very high levels of calcium compared to cortical and hippocampal plaques (Dhenain et al., 2002; Dhenain et al., 2009). Another study reported that amyloid plaques in APP/PS1 mice contain lower levels of iron and calcium than human AD plaques and even lower relative levels than surrounding tissue when normalized to protein content,

which they found to be higher in plaques (Leskovjan et al., 2009). This further supports our assertion that MR pulse sequences that rely heavily on the paramagnetic effects of iron should not be developed for plaque imaging in AD. Furthermore, if plaque-detecting pulse sequences are developed in AD transgenic mice rather than ex vivo human AD brain tissue, the pulse sequences may be even more sensitive to human AD plaques due to the added paramagnetic effects of higher levels of iron and other metals in the human AD plaques.

Since thalamic plaques contain much higher levels of iron, calcium, and other minerals and have a globular structure of concentric layers when viewed with electron microscopy (Dhenain et al., 2002; Dhenain et al., 2009), while cortical/hippocampal plaques have radially oriented fibrils (Sasaki et al., 2002), the Aβ and amyloid present in thalamic plaques may not have the same beta-sheet structure as cortical/hippocampal plaques. Differences in β-sheet structure and content might explain why the thalamic plaques stained intensely with the Aβ antibody, but not as intensely with thioflavine S, which binds to the beta-sheet structure of amyloid in general and not Aβ peptide specifically. In conclusion, the so-called thalamic plaques observed in APP/PS1 AD transgenic mice in the present study may not necessarily be unique to AD transgenic mouse models, but they appear to have no relation to the stereotypical senile/neuritic amyloid plaques in human AD patients or other transgenic mouse models. Therefore, we believe only (fibrillar) cortical and hippocampal plaques should be used as the endpoint for the development of MR imaging techniques to screen putative amyloid reducing/inhibiting therapies or, more importantly, for the detection of amyloid plaques and diagnosis of AD in human patients.

Summary

In summary, five-way anatomic spatial co-registration revealed that while iron plays a role in the detectability of amyloid plaques by MRI, cortical and hippocampal plaques have much lower levels of iron, but are still detectable by MRI, particularly T_2-weighted sequences, suggesting that other factors contribute to plaque detectability by MRI. Therefore, future studies of plaque deposition or therapeutic trials with secretase inhibitors or passive immunization using in vivo MRI plaque detection should use sequences that optimize the detectability of cortical and hippocampal plaques in mice because they more closely resemble human AD plaques, and focus less on sequences that rely solely on the magnetic susceptibility of iron. Pulse sequences such as the T_2SE pulse sequence used in the present study may be a good starting point. However, since T_2SE pulse sequences are also susceptible to iron paramagnetic effects and may detect any iron-containing structures such as blood vessels, microhemorrhages, and white matter in addition to plaques, the development of plaque specific contrast agents and MR pulse sequences that minimize magnetic susceptibility, such as T_1-weighted MR, should also be pursued to add a further level of confidence to the MR detection of amyloid plaques. In the interim, the present results make it highly encouraging to pursue the development of T_2-weighted spin-echo sequences for the detection of amyloid plaques in AD patients without the aid of a contrast-enhancing agent.

Research highlights

Human Alzheimer's disease (AD) and AD transgenic mouse amyloid plaques contain iron.

Many MR studies have attempted to image amyloid plaques using T2*-weighted pulse sequences that maximize the magnetic susceptibility effects of iron.

APP/PS1 transgenic mice develop two types of amyloid plaques based on histological and morphological analysis: 1) fibrillar, found predominantly in the cerebral cortex and hippocampus, and 2) spherical, found only in the thalamus.

Fibrillar plaques more closely replicate human AD amyloid plaques, but contain very low levels of iron and are much less detectable by T_2*-weighted MR.

T_2-weighted (spin echo) MR relies less on the magnetic susceptibility of iron and can detect fibrillar cortical and hippocampal amyloid plaques better than T_2*-weighted MR.

Acknowledgments

The authors would like to thank Karen Duff for providing the PS1 transgenic breeder mice, Gregor Adriany for developing the MRI coil, and Dawn Gregor and Jennifer Scott for their expert technical assistance. The authors would also like to thank Thomas Moyer, Ph.D. and Darcy Fjosne in the Metals Laboratory in the Mayo Dept. of Laboratory Medicine and Pathology. This work was supported by NIH grants R01 AG22034, P30 NS057091, and P41 RR008079, the Minnesota Biotechnology Partnership, the MIND Institute, and the Mayo Foundation.

References

Benveniste H, Einstein G, Kim KR, Hulette C, Johnson GA. Detection of neuritic plaques in Alzheimer's disease by magnetic resonance microscopy. Proc. Natl. Acad. Sci. USA 1999;96:14079–14084. [PubMed: 10570201]

Braak H, Braak E. Alzheimer's disease affects limbic nuclei of the thalamus. Acta Neuropathol 1991;81:261–268. [PubMed: 1711755]

Chamberlain R, Reyes D, Curran GL, Marjanska M, Wengenack TM, Poduslo JF, Garwood M, Jack CR Jr. Comparison of amyloid plaque contrast generated by T2-weighted, T2*-weighted, and susceptibility-weighted imaging methods in transgenic mouse models of Alzheimer's disease. Magn. Reson. Med 2009;61:1158–1164. [PubMed: 19253386]

Dhenain M, Privat N, Duyckaerts C, Jacobs RE. Senile plaques do not induce susceptibility effects in T_2*- weighted MR microscopic images. NMR Biomed 2002;15:197–203. [PubMed: 11968135]

Dhenain M, El Tannir El Tayara N, Wu TD, Guegan M, Volk A, Quintana C, Delatour B. Characterization of in vivo MRI detectable thalamic amyloid plaques from APP/PS1 mice. Neurobiol. Aging 2009;30:41–53. [PubMed: 17588710]

Falangola MF, Lee SP, Nixon RA, Duff K, Helpern JA. Histological co-localization of iron in A-beta plaques of PS/APP transgenic mice. Neurochem. Res 2005;30:201–205. [PubMed: 15895823]

Fujita N. Extravascular contribution of blood oxygenation level- dependent signal changes: A numerical analysis based on a vascular network model. Magn. Reson. Med 2001;46:723–734. [PubMed: 11590649]

Gerlach M, Ben-Shachar D, Riederer P, Youdim MB. Altered brain metabolism of iron as a cause of neurodegenerative diseases? J. Neurochem 1994;63:793–807. [PubMed: 7519659]

Haidarliu S, Ahissar E. Size gradients of barreloids in the rat thalamus. J. Comp. Neurol 2001;429:372–387. [PubMed: 11116226]

Helpern JA, Lee SP, Falangola MF, Dyakin VV, Bogart A, Ardekani B, Duff K, Branch C, Wisniewski T, de Leon MJ, Wolf O, O'Shea J, Nixon RA. MRI assessment of neuropathology in a transgenic mouse model of Alzheimer's disease. Magn. Reson. Med 2004;51:794–798. [PubMed: 15065253]

Hill JM, Switzer RC III. The regional distribution and cellular localization of iron in the rat brain. Neurosci 1984;11:595–603.

Holcomb L, Gordon MN, McGowan E, Yu X, Benkovic S, Jantzen P, Wright K, Saad I, Mueller R, Morgan D, Sanders S, Zehr C, O'Campo K, Hardy J, Prada CM, Eckman C, Younkin S, Hsiao K, Duff K. Accelerated Alzheimer-type phenotype in transgenic mice carrying both mutant amyloid precursor protein and presenilin 1 transgenes. Nat. Med 1998;4:97–100. [PubMed: 9427614]

Hsiao K, Chapman P, Nilsen S, Eckman C, Harigaya Y, Younkin S, Yang F, Cole G. Correlative memory deficits, A-beta elevation, and amyloid plaques in transgenic mice. Science 1996;274:99–102. [PubMed: 8810256]

Huang X, Moir RD, Tanzi RE, Bush AI, Rogers JT. Redox-active metals, oxidative stress, and Alzheimer's disease pathology. Ann. NY Acad. Sci 2004;1012:153–163. [PubMed: 15105262]

Irizarry MC, Locascio JJ, Hyman BT. Beta-site APP cleaving enzyme mRNA expression in APP transgenic mice: anatomical overlap with transgene expression and static levels with aging. Am. J. Pathol 2001;158:173–177. [PubMed: 11141490]

Jack CR Jr, Garwood M, Wengenack TM, Borowski BJ, Curran GL, Lin J, Adriany G, Grohn OHJ, Grimm R, Poduslo JF. In vivo visualization of Alzheimer's amyloid plaques by MRI in transgenic mice without a contrast agent. Magn. Reson. Med 2004;52:1263–1271. [PubMed: 15562496]

Jack CR Jr, Wengenack TM, Reyes DA, Garwood M, Curran GL, Borowski BJ, Lin J, Preboske GM, Holasek SS, Adriany G, Poduslo JF. In vivo magnetic resonance microimaging of individual amyloid plaques in Alzheimer's transgenic mice. J. Neurosci 2005;25:10041–10048. [PubMed: 16251453]

Koeppen AH. The history of iron in the brain. J. Neurol. Sci 1995;134 Suppl:1–9. [PubMed: 8847538]

Lee S-P, Falangola MF, Nixon RA, Duff K, Helpern JA. Visualization of amyloid plaques in a transgenic mouse model of Alzheimer's disease using MR microscopy without contrast reagents. Magn. Reson. Med 2004;52:538–544. [PubMed: 15334572]

Leskovjan AC, Lanzirotti A, Miller LM. Amyloid plaques in PSAPP mice bind less metal than plaques in human Alzheimer's disease. Neuroimage 2009;47:1215–1220. [PubMed: 19481608]

LeVine SM. Oligodendrocytes and myelin sheaths in normal, quaking, and shiverer brains are enriched in iron. J. Neurosci 1991;29:413–419.

LeVine SM. Iron deposits in multiple sclerosis and Alzheimer's disease brains. Brain Res 1997;760:298–303. [PubMed: 9237552]

Lovell MA, Robertson JD, Teesdale WJ, Campbell JL, Markesbery WR. Copper, iron, and zinc in Alzheimer's disease senile plaques. J. Neurol. Sci 1998;158:47–52. [PubMed: 9667777]

Mantyh PW, Ghilardi JR, Rogers S, DeMaster E, Allen CJ, Stimson ER, Maggio JE. Aluminum, iron, and zinc ions promote aggregation of physiological concentrations of beta-amyloid peptide. J. Neurochem 1993;61:1171–1174. [PubMed: 8360682]

McGowan E, Sanders S, Iwatsubo T, Takeuchi A, Saido T, Zehr C, Yu X, Uljon S, Wang R, Mann D, Dickson D, Duff K. Amyloid phenotype characterization of transgenic mice overexpressing both mutant amyloid precursor protein and mutant presenilin 1 transgenes. Neurobiol. Dis 1999;6:231–244. [PubMed: 10448051]

Miller LM, Wang Q, Telivala TP, Smith RJ, Lanzirotti A, Miklossy J. Synchrotron-based infrared and X-ray imaging shows focalized accumulation of Cu and Zn co-localized with β-amyloid deposits in Alzheimer's disease. J. Struc. Biol 2006;155:30–37.

Mitsumori F, Watanabe H, Takaya N, Garwood M. Apparent transverse relaxation rate in human brain varies linearly with tissue iron concentration at 4.7 T. Magn. Reson. Med 2007;58:1054–1060. [PubMed: 17969101]

Morris CM, Candy JM, Oakley AE, Bloxham CA, Edwardson JA. Histochemical distribution of non-haem iron in the human brain. Acta Anat 1992;144:235–257. [PubMed: 1529678]

Poduslo JF, Wengenack TM, Curran GL, Wisniewski T, Sigurdsson EM, Macura SI, Borowski BJ, Jack CR Jr. Molecular targeting of Alzheimer's amyloid plaques for contrast-enhanced magnetic resonance imaging. Neurobiol. Dis 2002;11:315–329. [PubMed: 12505424]

Robb, RA. A software system for interactive and quantitative analysis of biomedical images. In: Hohne, KH.; Fuchs, H.; Pizer, SM., editors. 3D Imaging in Medicine. Vol. 60. Berlin-Heidelberg: Springer Verlag; 1990. p. 333-361.

Sasaki A, Shoji M, Harigaya Y, Kawarabayashi T, Ikeda M, Naito M, Matsubara E, Abe K, Nakazato Y. Amyloid cored plaques in Tg2576 transgenic mice are characterized by giant plaques, slightly activated microglia, and the lack of paired helical filament-typed, dystrophic neurites. Virchows Archiv 2002;441:358–367. [PubMed: 12404061]

Schenck JF. Imaging of brain iron by magnetic resonance: T_2 relaxation at different field strengths. J. Neurol. Sci 1995;134 Suppl:10–18. [PubMed: 8847539]

Schultz C, Dick EJ, Cox AB, Hubbard GB, Braak E, Braak H. Expression of stress proteins alpha B-crystallin, ubiquitin, and hsp27 in pallido-nigral spheroids of aged rhesus monkeys. Neurobiol. Aging 2001;22:677–682. [PubMed: 11445268]

Smith MA, Perry G. Free radical damage, iron, and Alzheimer's disease. J. Neurol. Sci 1995;134 Suppl: 92–94. [PubMed: 8847550]

Vanhoutte G, Dewachter I, Borghgraef P, Van Leuven F, Van der Linden A. Non-invasive in vivo MRI detection of neuritic plaques associated with iron in APP[V717I] transgenic mice, a model for Alzheimer's disease. Magn. Reson. Med 2005;53:607–613. [PubMed: 15723413]

Vymazal J, Brooks RA, Patronas N, Hajek M, Bulte JW, Di Chiro G. Magnetic resonance imaging of brain iron in health and disease. J. Neurol. Sci 1995;134 Suppl:19–26. [PubMed: 8847541]

Wadghiri YZ, Sigurdsson EM, Sadowski M, Elliott JI, Li Y, Scholtzova H, Tang CY, Aguinaldo G, Pappolla M, Duff K, Wisniewski T, Turnbull DH. Detection of Alzheimer's amyloid in transgenic mice using magnetic resonance microimaging. Magn. Reson. Med 2003;50:293–302. [PubMed: 12876705]

Wadsworth PF, Jones HB, Cavanagh JB. The topography, structure and incidence of mineralized bodies in the basal ganglia of the brain of cynomolgus monkeys (Macaca fascicularis). Lab. Anim 1995;29:276–281. [PubMed: 7564211]

Wengenack TM, Whelan SL, Curran GL, Duff KE, Poduslo JF. Quantitative histological analysis of amyloid deposition in Alzheimer’s double transgenic mouse brain. Neurosci 2000;101:939–944.

Yablonskiy DA, Haacke EM. Theory of NMR signal behavior in magnetically inhomogeneous tissues: The static dephasing regime. Magn. Reson. Med 1994;32:749–763. [PubMed: 7869897]

Yanai T, Masegi T, Ueda K, Manabe J, Teranishi M, Takaoka M, Matsunuma N, Fukuda K, Goto N, Fujiwara K. Vascular mineralization in the monkey brain. Vet. Pathol 1994;31:546–552. [PubMed: 7801432]

Zhang J, Yarowsky P, Gordon MN, Di Carlo G, Munireddy S, van Zijl PC, Mori S. Detection of amyloid plaques in mouse models of Alzheimer’s disease by magnetic resonance imaging. Magn. Reson. Med 2004;51:452–457. [PubMed: 15004784]

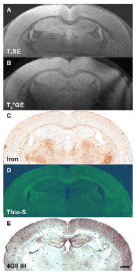

Fig. 1.

Five-way anatomic spatial co-registration of a 9-month old APP/PS1 AD transgenic mouse brain. Ex vivo MRI scans of matched sections imaged using either a (A) T_2SE or (B) T_2*GE pulse sequence. Matched adjacent histological sections processed with (C) DAB-enhanced iron staining, (D) thioflavine S amyloid staining, or (E) anti-Aβ peptide immunohistochemistry. Scale bar = 500 μm.

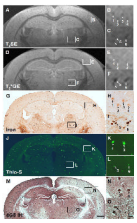

Fig. 2.

Five-way anatomic spatial co-registration of a 12-month old APP/PS1 AD transgenic mouse brain. Ex vivo MRI scans of matched sections imaged using either a (A) T_2SE or (D) T_2*GE pulse sequence. Matched adjacent histological sections processed with (G) DAB-enhanced iron staining, (J) thioflavine S amyloid staining, or (M) anti-Aβ peptide immunohistochemistry. Scale bar = 500 μm. (B, E, H, K, and N) Higher magnification of cortical plaques positively matched by spatial co-registration. Corresponding plaques are labeled with numbers when present in a particular section. All matched plaques may not be present in all adjacent histological sections. (C, F, I, L, and O) Higher magnification of thalamic plaques positively matched by spatial co-registration. (O) Scale bar = 100 μm.

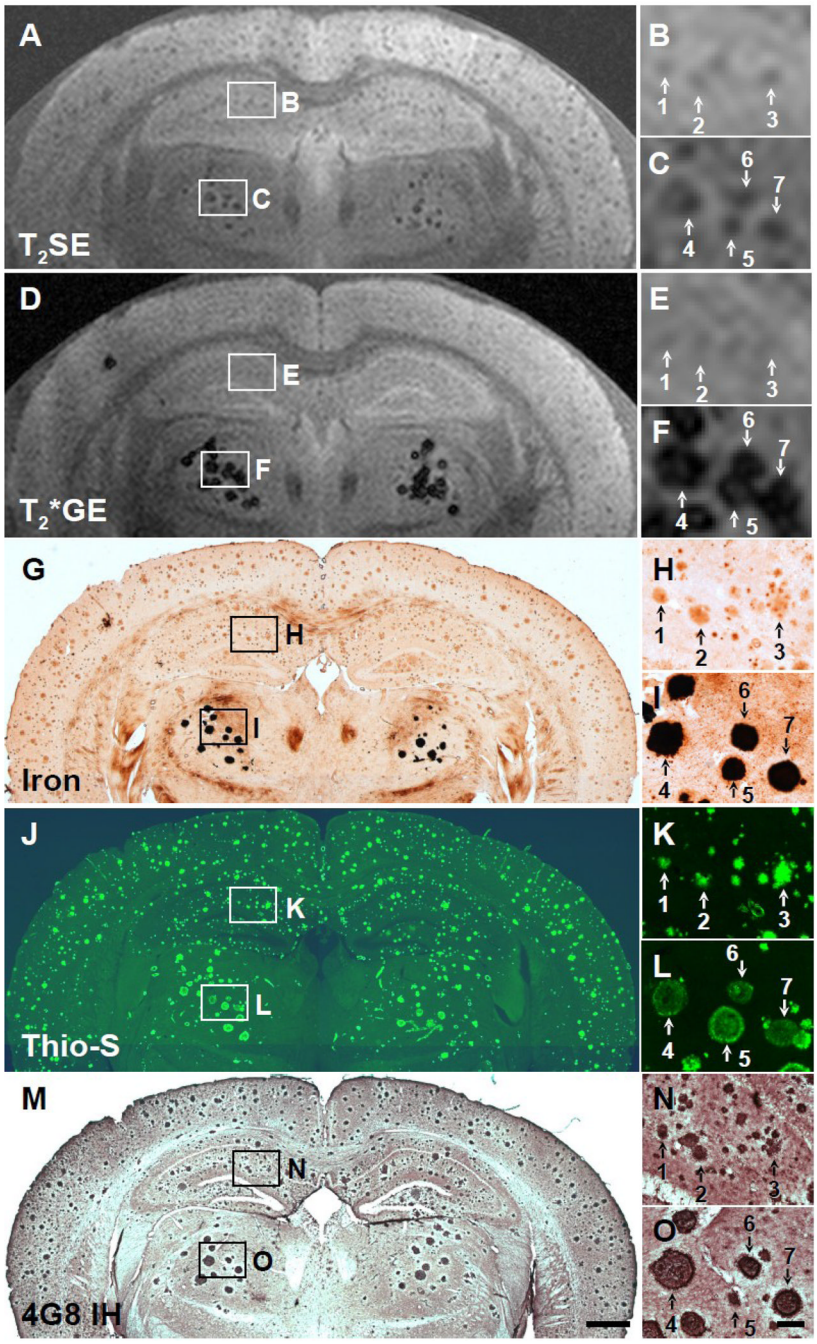

Fig. 3.

Five-way anatomic spatial co-registration of a 24-month old APP/PS1 AD transgenic mouse brain. Ex vivo MRI scans of matched sections imaged using either a (A) T_2SE or (D) T_2*GE pulse sequence. Matched adjacent histological sections processed with (G) DAB-enhanced iron staining, (J) thioflavine S amyloid staining, or (M) anti-Aβ peptide immunohistochemistry. Scale bar = 500 μm. (B, E, H, K, and N) Higher magnification of hippocampal plaques positively matched by spatial co-registration. Corresponding plaques are labeled with numbers when present in a particular section. (C, F, I, L, and O) Higher magnification of thalamic plaques positively matched by spatial co-registration. (O) Scale bar = 100 μm.

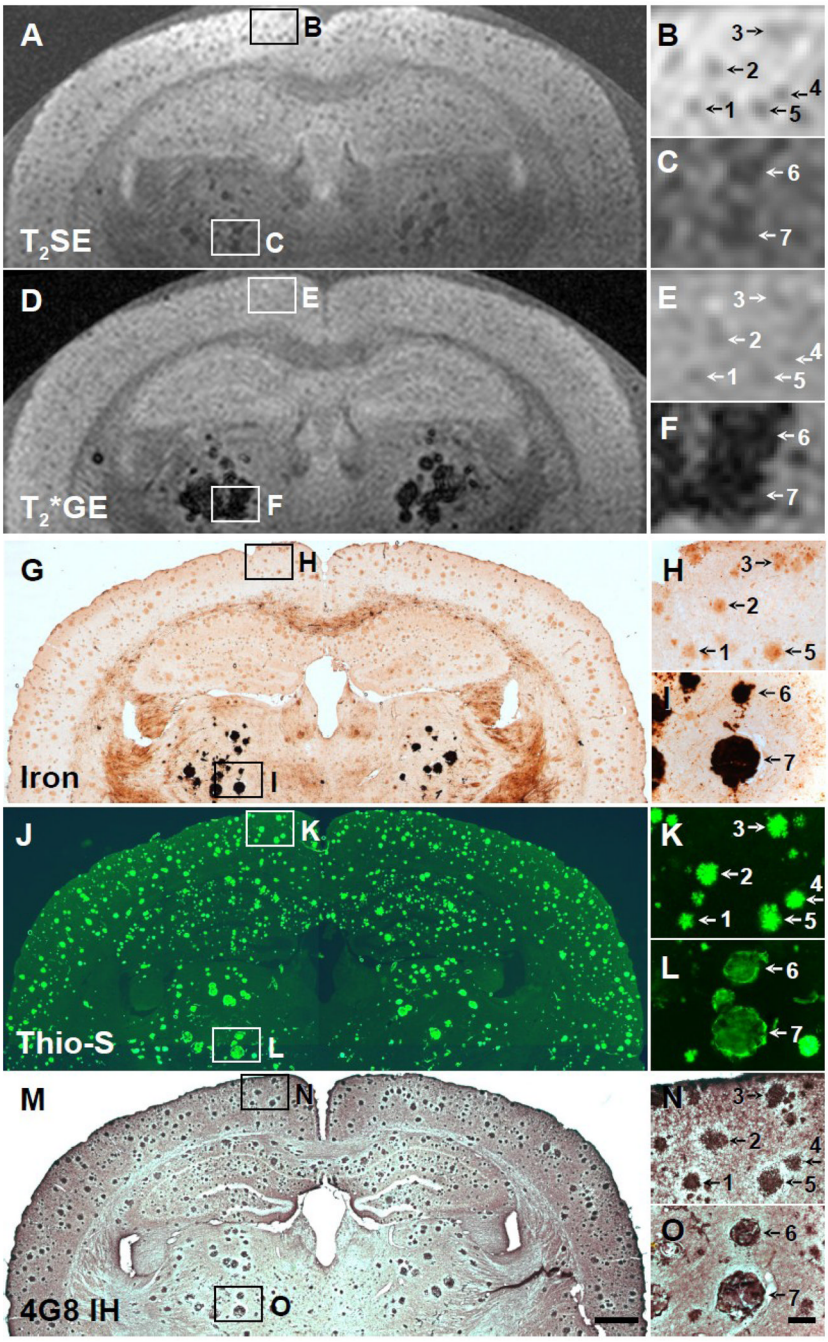

Fig. 4.

Five-way anatomic spatial co-registration of a 30-month old APP/PS1 AD transgenic mouse brain. Ex vivo MRI scans of matched sections imaged using either a (A) T_2SE or (D) T_2*GE pulse sequence. Matched adjacent histological sections processed with (G) DAB-enhanced iron staining, (J) thioflavine S amyloid staining, or (M) anti-Aβ peptide immunohistochemistry. Scale bar = 500 μm. (B, E, H, K, and N) Higher magnification of cortical plaques positively matched by spatial co-registration. Corresponding plaques are labeled with numbers when present in a particular section. All matched plaques may not be present in all adjacent histological sections. (C, F, I, L, and O) Higher magnification of thalamic plaques positively matched by spatial co-registration. (O) Scale bar = 100 μm.

Table 1

Densitometry of plaques and tissue in APP/PS1 and WT brain sections stained for iron.

Region	APP/PS1 APP/PS1 Tiss. vs. Plaque[a]	APP/PS1 Tissue[a]	Plaq./Tiss. Ratio	APP/PS1 Plaq. vs Tiss p-value[b]	WT Tissue[a]
	WT Tiss. p-value [c]				
Cortex	153.6 ± 2.6 ns	222.8 ± 1.8	0.69 ± 0.01	0.001	219.2 ± 0.4
Hippocampus	153.8 ± 2.8 ns	218.7 ± 1.0	0.70 ± 0.01	0.001	215.9 ± 0.8
Thalamus	11.8 ± 0.2 0.001	215.7 ± 2.1	0.055 ± 0.001	0.001	201.4 ± 1.4

[a] Mean (± SEM) gray level value of n=10 plaques or adjacent tissue ROIs per region measured in 8-bit gray scale images of DAB-enhanced Prussian blue stained histological sections from a 24-month old APP/PS1 or age-matched WT mouse. Lower gray level value indicates darker staining and relatively higher iron content.

[b] Two-way ANOVA APP/PS1 Plaque vs. Tissue Iron Densitometry: Plaque vs. Tissue – $F(1,59)=4874.35$, $p<0.001$; Region - $F(2,59)=921.83$, $p<0.001$; Plaq./Tiss. × Reg. Interaction – $F(2,59)=799.64$, $p<0.001$; Student-Newman-Keuls multiple comparisons.

[c] Two-way ANOVA APP/PS1 Tissue vs. WT Tissue Iron Densitometry: AD vs. WT – $F(1,59)=37.13$, $p<0.001$; Region - $F(2,59)=42.50$, $p<0.001$; AD/WT × Reg. Interaction – $F(2,59)=10.72$, $p<0.001$; Student-Newman-Keuls multiple comparisons.

Table 2

Total iron content of fresh brain tissue in APP/PS1 and WT mice.

Brain Region	APP/PS1[a]	WT[a]	APP/PS1 vs. WT p-value[b]
Cortex	15.00 ± 1.10	11.45 ± 0.05	ns
Hippocampus	13.20 ± 0.50	10.90 ± 3.68	ns
Thalamus	20.00 ± 0.40	11.80 ± 1.60	0.005

[a] Mean (± SEM) tissue iron (μg/g tissue) measured by inductively coupled plasma – mass spectrometry (ICP-MS).

[b] Two-way ANOVA APP/PS1 vs. WT Tissue Iron: APP/PS1 vs. WT – [$F(1,11)=18.04$, $p<0.005$]; Brain Region – [$F(2,11)=4.27$, $p<0.07$]; APP/PS1 vs. WT × Region Interaction – [$F(2,11)=2.65$, ns]; Student-Newman-Keuls post-hoc multiple comparisons.